Sound-Horizon-Agnostic Inference of the Hubble Constant and Neutrino Mass from BAO, CMB Lensing, and Galaxy Weak Lensing and Clustering

Helena García Escudero[**]

Center for Cosmology, Department of Physics and Astronomy,
University of California, Irvine, California 92697-4575, USA

Seyed Hamidreza Mirpoorian[*][†] and Levon Pogosian[‡]

Department of Physics, Simon Fraser University, Burnaby, British Columbia, Canada V5A 1S6

We present a sound-horizon-agnostic determination of the Hubble constant, H_0, by combining DESI DR2 baryon acoustic oscillation (BAO) data with the latest cosmic microwave background (CMB) lensing measurements from Planck, ACT, and SPT-3G, the angular size of the CMB acoustic scale, Dark Energy Survey Year-3 (3×2-pt) galaxy weak lensing and clustering correlations, and the Pantheon+ supernova sample. In this analysis, the sound horizon at the drag epoch, r_d, is treated as a free parameter, avoiding assumptions about early-Universe physics. By combining uncalibrated comoving distances from BAO and supernovae with constraints on the matter density $\Omega_m h^2$ from CMB and galaxy lensing/clustering, we break the r_d–H_0 degeneracy and obtain $H_0 = 70.0 \pm 1.7$ km/s/Mpc when the sum of the neutrino masses is fixed at $\Sigma m_\nu = 0.06$ eV. With a conservative prior on the amplitude of primordial fluctuations, A_s, we find $H_0 = 70.03 \pm 0.97$ km/s/Mpc and $r_d = 144.8 \pm 1.6$ Mpc. Allowing Σm_ν to vary yields $H_0 = 75.3^{+3.3}_{-4.0}$ km/s/Mpc and $\Sigma m_\nu = 0.55^{+0.23}_{-0.37}$ (< 1.11 eV) at 68% (95%) CL, and $H_0 = 73.9 \pm 2.2$ km/s/Mpc with $\Sigma m_\nu = 0.46^{+0.21}_{-0.25}$ ($= 0.46^{+0.40}_{-0.45}$ eV) at 68% (95%) CL when a prior on A_s is applied. Forecasts for the completed DESI BAO program, combined with Simons-Observatory-like CMB lensing, next-generation 3×2-pt data, and expanded supernova samples predict $\sigma(H_0) \simeq 0.67$ km/s/Mpc with fixed Σm_ν, and $\sigma(H_0) \simeq 1.1$ km/s/Mpc with $\Sigma m_\nu < 0.133$ (< 0.263) eV at 68% (95%) CL when the neutrino mass is varied. As the precision of BAO, CMB lensing, and galaxy lensing/clustering improve, this r_d-agnostic framework will provide an independent test of the need for new physics at recombination.

I. INTRODUCTION

Determining the Hubble constant, H_0, with high precision is both a fundamental goal and an ongoing challenge in modern cosmology. Despite the success of the standard ΛCDM model in explaining a wide range of cosmological observations, a significant tension persists between the value $H_0 = 67.36 \pm 0.54$ km/s/Mpc inferred from *Planck* measurements of the cosmic microwave background (CMB), under the assumption of ΛCDM [1], and the value $H_0 = 73.04 \pm 1.04$ km/s/Mpc obtained from Cepheid-based distance ladder measurements [2].

CMB analyses rely on the well-established physics of recombination to determine the sound horizon at photon–baryon decoupling, or the drag epoch, r_d, which is used in the extraction of cosmological parameters. However, the Hubble tension may indicate the need for additional physics during the epoch of recombination, such as primordial magnetic fields [3–6], early dark energy [7–9], extra relativistic species [10, 11], neutrino self-interactions [12, 13], or variations of fundamental constants that alter recombination physics [14–16], among other proposed mechanisms [17–19]. These scenarios

would modify the standard determination of r_d, making it smaller and thereby increasing the CMB-inferred value of H_0.

This motivates the exploration of methods for constraining H_0 that do not rely on modeling r_d. Several recent studies [20–25] have utilized datasets that probe the scale of matter–radiation equality, $k_{\rm eq}$, and hence the physical matter density $\Omega_m h^2$, in combination with uncalibrated supernova (SN) luminosity distances, which constrain the present-day matter fraction Ω_m, to obtain a sound-horizon-free measurement of H_0. Both the full-shape galaxy power spectrum $P(k)$ and the CMB lensing convergence spectrum $C_\ell^{\kappa\kappa}$ are sensitive to $k_{\rm eq}$. In full-shape analyses, $P(k)$ is decomposed into its smooth (the component that constrains $k_{\rm eq}$) and oscillatory (BAO) parts, and r_d is marginalized over in the oscillatory part to eliminate dependence on the sound horizon. While this method preserves some of the calibration-independent angular diameter distance information encoded in the BAO wiggles, it does not fully exploit the constraining power of the complete set of transverse, radial, and volume-averaged BAO observables.

In this work, we employ an alternative approach introduced in [26], combining uncalibrated transverse, radial, and volume-averaged BAO measurements, which constrain $r_d H_0$ and Ω_m, with CMB and galaxy lensing, which provide a constraint on $\Omega_m h^2$ and break the r_d–H_0 degeneracy. Here, r_d is treated as a free primary parameter and is measured from the data alongside H_0. We use BAO measurements from the DESI

---

[*] garciaeh@uci.edu
[†] smirpoor@sfu.ca
[‡] levon@sfu.ca
  [*]These authors contributed equally to this work and are listed alphabetically by last name.

DR2 release [27], the combination [25] of CMB lensing convergence spectra $C_\ell^{\kappa\kappa}$ from *Planck* [28], the Atacama Cosmology Telescope (ACT DR6) [29–31], and the South Pole Telescope (SPT-3G) [32], hereafter referred to as APS, along with the DES Year-3 three two-point galaxy weak lensing and clustering correlation functions (3×2-pt, DESY3) [33, 34]. In addition, we include the CMB acoustic scale angle, $\theta_\star$, treating it as an additional transverse BAO point at redshift $z = 1090$. We also include the Pantheon+ compilation of uncalibrated SN magnitudes [35], which add an additional constraint on Ω_m; however, this contribution is not significant since the uncalibrated BAO data alone already constrain Ω_m well.

In addition to providing an early-Universe-independent constraint on H_0, our approach also enables, in principle, a measurement of the sum of neutrino masses, Σm_ν, through the sensitivity of CMB lensing and galaxy lensing and clustering to the suppression of small-scale structure, especially when combined with a weak external prior on the amplitude of primordial fluctuations A_s. By combining DESI DR2 BAO and $\theta_\star$ with CMB lensing from APS, DESY3 galaxy weak lensing and clustering, and the Pantheon+ SN, we obtain $H_0 = 70.0 \pm 1.7$ km/s/Mpc when Σm_ν is fixed at the minimal value of 0.06 eV. With an additional conservative but informative prior on A_s, we obtain $H_0 = 70.03 \pm 0.97$ km/s/Mpc and $r_d = 144.8 \pm 1.6$ Mpc. Allowing Σm_ν to vary, we find $H_0 = 75.3^{+3.3}_{-4.0}$ km/s/Mpc and $\Sigma m_\nu < 1.11$ eV (95% CL) without an informative prior on A_s, and $H_0 = 73.9 \pm 2.2$ km/s/Mpc with $\Sigma m_\nu = 0.46^{+0.40}_{-0.45}$ eV (95% CL) when the prior on A_s is included. We also perform forecasts showing that future CMB lensing data from a Simons-Observatory-like (SO-L) experiment [36] and future galaxy weak lensing and clustering measurements, when combined with data from the completed DESI BAO program and an expanded SN dataset, can constrain H_0 with a precision of ~ 0.67 km/s/Mpc if Σm_ν is fixed, and ~ 1.1 km/s/Mpc when Σm_ν is varied, with $\Sigma m_\nu < 0.26$ eV (95% CL).

The structure of this paper is as follows: Section II introduces our approach to using the BAO observables in an r_d-independent way and discusses the sensitivity of the datasets used in this analysis to the parameters of interest. Section III A presents the details of the analysis, including the data likelihoods, parameter prior assumptions, and the forecast methodology. In Section IV, we present the constraints derived from current data and the forecasts, with and without varying Σm_ν. We summarize our findings in Section V.

II. CONSTRAINING COSMOLOGY WITH THE SOUND HORIZON AS A FREE PARAMETER

A. BAO Observables

BAO provide standard-ruler distance measurements through three types of observables [37]: the transverse

BAO scale, the line-of-sight BAO scale, and the isotropic average of the two. The transverse observable measures the angular size of the sound horizon r_d and is defined as

$$\beta_\perp(z) = \frac{D_M(z)}{r_d}, \quad (1)$$

where $D_M(z)$ is the comoving distance to redshift z. For illustration, we focus on $\beta_\perp(z)$, though the methodology described below applies equally to the radial and isotropic BAO observables.

Assuming a spatially flat ΛCDM model and neglecting radiation (an acceptable approximation at the relevant redshifts), $\beta_\perp(z)$ can be written as

$$\begin{aligned} \beta_\perp(z) &= \frac{1}{r_d} \int_0^z \frac{c\,dz'}{H(z')} \\ &= \frac{2998\,\text{Mpc}}{r_d h} \int_0^z \frac{dz'}{\sqrt{\Omega_m(1+z')^3 + (1-\Omega_m)}}, \quad (2) \end{aligned}$$

where $c/H_0 = 2998\,\text{Mpc}/h$, and $h = H_0/(100\,\text{km/s/Mpc})$. This shows that BAO observations at multiple redshifts constrain both the matter density fraction Ω_m and the product $r_d h$. Breaking the degeneracy between r_d and h requires additional information, such as the standard-model prediction for r_d combined with a Big Bang Nucleosynthesis (BBN) prior on the baryon density ω_b [38]. An alternative, explored in [26, 39] and adopted here, is to supplement BAO with a constraint on $\Omega_m h^2$ while treating r_d as a free parameter, thereby avoiding assumptions about the sound horizon.

The additional constraint on $\Omega_m h^2$ can come from CMB lensing measurements, which are sensitive to the matter–radiation equality scale k_{eq} and thus constrain the matter-to-radiation density ratio. As a consistency test, one may also adopt a Gaussian prior on $\Omega_m h^2$ from the Planck best-fit ΛCDM model and check whether the H_0 and r_d values inferred from BAO agree with those in the best-fit model [26, 39].

Unlike full-shape $P(k)$ approaches [20, 23, 24], this method makes use of all three BAO observables at each redshift, maximizing the geometrical information encoded in the data. In particular, it enables a constraint on H_0 that is less dependent on SN-derived values of Ω_m, since BAO alone already provide a strong constraint.

Finally, one can include the CMB acoustic scale angle, $\theta_\star$, treating it as an additional transverse BAO data point at $z = 1100$, as discussed in Sec. III A 2.

B. CMB Lensing, Galaxy Lensing and Clustering

The matter–radiation equality scale is imprinted in the matter power spectrum, which determines the CMB lensing convergence spectrum $C_\ell^{\kappa\kappa}$. As shown in [21, 40], CMB lensing constrains the combination $A_s(\Omega_m h^2)^\alpha$, where $\alpha > 0$. Owing to projection effects, $C_\ell^{\kappa\kappa}$ is nearly

insensitive to the acoustic oscillation features in $P(k)$, and hence to the value of r_d, as we demonstrate below. However, CMB lensing does depend on the baryon fraction of the total matter density, since baryons cluster later than dark matter and their abundance affects the growth factor. For this reason, even though we treat r_d as a free parameter, we still apply the BBN prior on ω_b.
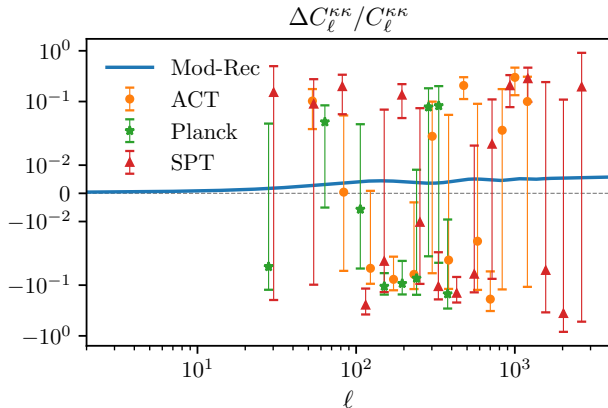

Figure 1: Relative difference in the CMB lensing convergence spectrum $C_\ell^{\kappa\kappa}$ for a modified recombination model with an r_d smaller by 2%, relative to the Planck best-fit ΛCDM model. Orange points, green stars, and red triangles with error bars show the $C_\ell^{\kappa\kappa}$ bandpowers from *ACT*, *Planck*, and *SPT-3G*, respectively. The figure illustrates that recombination changes capable of raising H_0 to ~ 72 km/s/Mpc have only a minor effect on the CMB lensing spectrum.

The late-time matter distribution can also be probed through galaxy clustering and galaxy weak lensing, which depend on both the amplitude and scale-dependence of matter fluctuations. These observables provide complementary information to CMB lensing. The three two-point correlation functions (3×2-pt) are

$$w_{ij}(\theta) = \langle \delta_g^i(\hat{n}) \, \delta_g^j(\hat{n}+\theta)\rangle, \qquad (3)$$

$$\gamma_{t,ij}(\theta) = \langle \delta_g^i(\hat{n}) \, \gamma_t^j(\hat{n}+\theta)\rangle, \qquad (4)$$

$$\xi_{\pm,ij}(\theta) = \langle \gamma^i(\hat{n}) \, \gamma^j(\hat{n}+\theta)\rangle, \qquad (5)$$

where δ_g^i is the galaxy overdensity in redshift bin i, γ_t^j is the tangential shear in bin j, and γ^i is the shear field. In this work, we include all three correlation functions.

To assess the sensitivity of CMB lensing and galaxy 3×2-pt data to the sound horizon, we compared observables computed with the standard ionization history $x_e(z)$ in the Planck best-fit ΛCDM cosmology to those obtained with the same cosmological parameters but a modified $x_e(z)$. Specifically, we used the four-parameter phenomenological model of [41], which yields an r_d smaller by about 2%, corresponding to $H_0 \sim 72$ km/s/Mpc. Figure 1 shows the resulting relative difference in $C_\ell^{\kappa\kappa}$, alongside lensing bandpowers from Planck,

ACT-DR6, and SPT-3G. The change remains below 1% and well within current measurement uncertainties. Similarly, Fig. 2 shows the residuals in $w_{ij}(\theta)$ and $\gamma_{t,ij}(\theta)$, compared to DES Y3 measurements [33, 42]. For brevity, $\xi_{\pm,ij}(\theta)$ is not shown, as it also exhibits no significant difference. These comparisons demonstrate that CMB lensing and galaxy 3×2-pt observables are effectively insensitive to moderate reductions in r_d induced by modified recombination physics.

C. The effect of massive neutrinos

Massive neutrinos affect both the expansion history and the growth of cosmic structures. Neutrinos with total mass $\Sigma m_\nu \lesssim 1$ eV behave as relativistic species before photon–baryon decoupling, contributing to the radiation energy density at $z \gtrsim 1000$ and delaying matter–radiation equality. This alters the horizon scale at equality, $k_{\rm eq}$, imprinted in the matter power spectrum. On smaller scales, neutrino free-streaming suppresses the growth of density fluctuations below the free-streaming length, producing a scale-dependent suppression of the matter power spectrum. Both effects influence the CMB lensing convergence spectrum, modifying its amplitude and shape, as shown in Fig. 2 of [43]. Combining CMB lensing with other cosmological probes that constrain the present-day matter density fraction therefore provides sensitivity to the neutrino mass (see, e.g., [43–45]).

The 3×2-pt galaxy weak lensing and clustering data, such as DES measurements, constrain the clustering amplitude and expansion history at low redshift, strengthening joint inference and significantly reducing the allowed parameter space for neutrino masses. Massive neutrinos suppress small-scale power and lower the amplitude of clustering and shear correlations, while the altered growth history modifies their redshift evolution. Because galaxy weak lensing and clustering respond differently to changes in the growth of structure and in Ω_m, their combination provides complementary sensitivity to Σm_ν through both scale-dependent suppression and changes in Ω_m.

D. Parameter degeneracies

In ΛCDM, BAO constrain $r_d H_0$ and Ω_m, while the CMB lensing spectrum amplitude constrains approximately (see Eq. (2.10) of Craig *et al.* [45])

$$C_\ell^{\kappa\kappa} \propto (\Omega_m h^2)^2 A_s \left[1 - 0.003 \frac{\Sigma m_\nu/(58 \text{ meV})}{\Omega_m h^2}\right]. \quad (6)$$

This scaling shows that, even if the neutrino fraction is known, external information on A_s is needed to determine $\Omega_m h^2$. With Σm_ν free, the CMB lensing amplitude alone cannot disentangle $\Omega_m h^2$, A_s, and f_ν. An additional constraint on Σm_ν comes from the scale-dependent
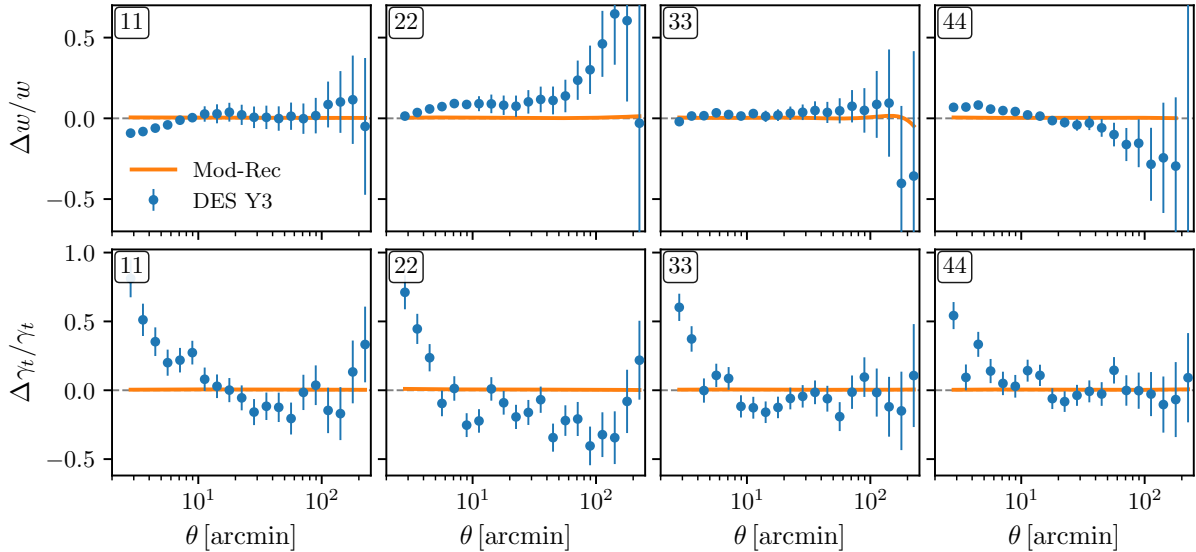
Figure 2: Relative difference with respect to the Planck+DES Y3 best-fit ΛCDM prediction for galaxy clustering correlation functions $w_{ij}(\theta)$ and $\gamma_{t,ij}(\theta)$ in four redshift bins ($i = j = 1, \ldots, 4$). Points with error bars show the DES Y3 measurements, while solid lines show the residuals for the same modified recombination model as in Fig. 1. The figure shows that recombination changes leave the 3×2-pt observables essentially unaffected.

suppression of $C_\ell^{\kappa\kappa}$, illustrated in Fig. 2 of [43]. The detectability of this suppression depends on the noise in $C_\ell^{\kappa\kappa}$. Including galaxy lensing and clustering extends the mode coverage and enhances the ability to disentangle $\Omega_m h^2$, A_s, and Σm_ν. In addition, A_s is well constrained by large-scale CMB anisotropies, which are independent of r_d, justifying the adoption of a conservative prior on A_s from CMB data (see Sec. III B).

Allowing for massive neutrinos, which contribute as radiation at equality but as part of Ω_m today, introduces a positive correlation between Σm_ν and H_0 when using CMB lensing and BAO. A larger Σm_ν reduces the effective matter density at equality, requiring a larger $\Omega_m h^2$ to maintain the same $k_{\rm eq}$. With Ω_m constrained by BAO, this in turn requires a larger H_0. These parameter relationships are evident in Fig. 3, which shows the joint posteriors for H_0, Σm_ν, and $\Omega_m h^2$ (see also Fig. 2 of [43]).

III. ANALYSIS DETAILS

A. Datasets

1. DESI DR2 BAO

We use the DESI DR2 BAO `Cobaya` likelihood, based on measurements provided in Table III of [27]. The dataset includes the D_V/r_d measurement from the BGS sample at $0.1 < z < 0.4$, D_M/r_d and D_H/r_d for two LRG bins at $0.4 < z < 0.6$ and $0.6 < z < 0.8$, a combined

LRG+ELG tracer at $0.8 < z < 1.1$, ELG measurements at $1.1 < z < 1.6$, QSO clustering BAO at $0.8 < z < 2.1$, and the Lyα BAO constraint at $1.8 < z < 4.2$. We refer to this dataset as DESI2.

2. The CMB acoustic scale $\theta_\star$

The CMB acoustic scale angle, $\theta_\star$, also known as $\theta_{\rm CMB}$, is the angular size of the sound horizon at the epoch of recombination. We use $\theta_\star$ as a transverse BAO measurement, $\beta_\perp^\star = 94.286 \pm 0.217$, at $z_\star = 1090$ [39], derived from $\theta_\star$ measured by Planck under the assumption that the ΛCDM relation between r_d and the sound horizon at the redshift corresponding to the peak of the CMB visibility function, $r_\star$, holds (with $r_\star \approx r_d/1.02$). The authors verified that this relation remains valid in known extensions of ΛCDM that modify r_d.

Adding $\theta_\star$ to our dataset helps tighten the BAO constraints on $r_d H_0$ and Ω_m.

3. CMB Lensing: Planck, ACT, and SPT-3G

We use the combination of CMB lensing bandpowers from *Planck* [28], the Atacama Cosmology Telescope (ACT DR6) [29–31], and the South Pole Telescope (SPT-3G) [32] provided in [25]. This combination, subsequently referred to as APS-L, provides the most constraining CMB lensing power spectrum measurement to date with a combined signal-to-noise ratio of 61, offering

strong constraints on the amplitude of matter fluctuations S_8 [25].

4. *Dark Energy Survey* 3×2-*pt*

We include the full 3×2-pt correlation functions from the Dark Energy Survey Year 3 (DES Y3) encompassing cosmic shear, galaxy clustering, and galaxy-galaxy lensing as detailed in [33]. This joint analysis over ~ 5000 deg^2 provides competitive constraints on cosmological parameters, yielding $S_8 = 0.776^{+0.017}_{-0.017}$ and $\Omega_m = 0.339^{+0.032}_{-0.031}$, and serves as a powerful low-redshift complement to CMB-based probes. By directly tracing the growth of structure, DES Y3 measurements are particularly sensitive to the suppression effects induced by massive neutrinos, thereby providing valuable information on the sum of neutrino masses. We use the `Cobaya` [46] implementation of the likelihood from [47].

5. *Pantheon+ Supernovae*

We use the Pantheon+ (PP) dataset of 1550 spectroscopically-confirmed Type Ia SN spanning $0.001 < z < 2.26$ to probe the late-time expansion history [35, 48]. This updated compilation improves upon the original Pantheon release through enhanced photometric calibration, extended low-redshift coverage, and refined treatment of systematics.

B. Model Parameters and Priors

We use the Monte-Carlo Markov Chains (MCMC) package `Cobaya` [46] with a version of the Boltzmann code `CAMB` [49] modified to treat r_d as a primary (rather than derived) parameter. The sampled parameters are r_d, H_0, $\Omega_c h^2$, $\Omega_b h^2$, the spectral index n_s, A_s, and Σm_ν. We also consider the case where Σm_ν is fixed at the minimal value of 0.06 eV. The parameter priors adopted in this work are summarized in Table I. Below, we briefly explain the reasoning behind our choices of priors.

For the H_0 and the cold dark matter density parameter, $\Omega_c h^2$, we use flat uninformative priors with ranges given in Table I.

When analysing the current data, we present results both with a weak flat prior on A_s, $\ln(10^{10}A_s) \in [2, 4]$ (same as in [25]), as well a Gaussian prior, $\mathcal{N}(3.04, 0.02)$, centered on the Planck-ΛCDM preferred value [50] with a standard deviation encompassing the A_s posteriors obtained in a broad range of modified recombination models [41]. Having a stronger prior on A_s helps break the degeneracy between A_s and $\Omega_m h^2$ in CMB lensing, significantly tightening the posterior of H_0.

For the scalar spectral index n_s, we adopt a Gaussian prior $\mathcal{N}(0.96, 0.02)$, same as the prior used in [25], that encompasses a broad range of posteriors in models with

	Current Data	Forecast
	Prior	Fiducial value, Prior
$\ln(10^{10}A_s)$	[2, 4] or $\mathcal{N}(3.04, 0.02)$	3.045, $\mathcal{N}(3.04, 0.02)$
H_0 [km/s/Mpc]	[40, 100]	67.32, [40, 100]
n_s	$\mathcal{N}(0.96, 0.02)$	0.966, $\mathcal{N}(0.96, 0.02)$
$100\,\Omega_b h^2$	$\mathcal{N}(2.23, 0.05)$	2.24, $\mathcal{N}(2.23, 0.05)$
$\Omega_c h^2$	[0.001, 0.99]	0.120, [0.001, 0.99]
Σm_ν [eV]	[0, 3.0]	0.06, [0, 3.0]
r_d [Mpc]	[100, 200]	147.1, [100, 200]
τ (fixed)	0.059	0.059

Table I: Priors adopted for the parameters in the analysis of current data, and the fiducial values and priors used in the forecast. Uniform priors are indicated by square brackets, while Gaussian priors with mean μ and standard deviation σ are denoted as $\mathcal{N}(\mu, \sigma)$.

modified recombination histories. We found that adopting a more restrictive prior on n_s did not appreciably alter the constraints on the parameters of interest.

Varying the optical depth to reionization, τ, has no impact on our posterior distributions. We therefore fix this parameter to the Planck + DESI DR2 ΛCDM best-fit value, $\tau = 0.059$ [51]. This choice is also consistent with the value obtained from the `SRoll2` low-ℓ polarization analysis [52]. Given the key role of τ for the parameter constraints derived from the combination of CMB temperature, polarization and lensing spectra, with implications for the apparent tension between the Planck CMB and DESI BAO [53], having a τ-insensitive way of measuring a subset of cosmological parameters offers a valuable cross-check.

We adopt a Gaussian prior on the physical baryon density, $\Omega_b h^2 \sim \mathcal{N}(0.0223, 0.0005)$, obtained from observations of the primordial abundances of light elements, particularly deuterium, and is consistent with the standard BBN scenario combined with updated nuclear reaction rate data [54].

We adopt a wide and minimally informative flat prior on the net neutrino mass, Σm_ν, spanning $[0, 3]$ eV, allowing our constraints to remain largely driven by the data [11]. We also perform separate analyses with Σm_ν fixed at the minimum value of 0.06 eV determined by neutrino oscillation experiments [55–59]. We note that prior choice for the neutrino mass sum has been shown to significantly affect Bayesian evidence and posterior inferences, especially in the case of signigicant parameter degeneracies. Several works have emphasized the impact of adopting linear versus logarithmic priors, particularly in distinguishing between neutrino mass orderings and assessing constraints on Σm_ν [60–64]. In light of these findings, our baseline analysis adopts a uniform prior on Σm_ν, consistent with common practice in cosmological analyses. However, we also demonstrate in Fig. 4 the

impact of using a logarithmic prior. In addition, a number of groups have explored analyses where Σm_ν is allowed to take negative values, which can be informative for isolating parameter degeneracies and quantifying the statistical power of cosmological data [43, 45, 65]. Investigating negative-mass parameterizations lies beyond the scope of this project.

C. Forecasts

In what follows, we describe the methodology used in our forecasts of the constraints expected from future CMB lensing, galaxy lensing and clustering, BAO and SN datasets. We adopt the Planck best-fit ΛCDM model as our fiducial cosmology with parameters provided in Table I.

1. CMB Lensing

For the forecast, we construct a lensing likelihood function $\mathcal{L}$ assuming Gaussian errors and covariance for the binned CMB lensing convergence spectrum, $\hat{C}_{L_b}^{\kappa\kappa}$ [29, 31]:

$$-2\ln\mathcal{L} = \Sigma_{bb'}\left[\hat{C}_{L_b}^{\kappa\kappa} - C_{L_b}^{\kappa\kappa}(\theta)\right]\mathbb{C}_{bb'}^{-1}\left[\hat{C}_{L_b'}^{\kappa\kappa} - C_{L_b'}^{\kappa\kappa}(\theta)\right],$$

(7)

where b denotes a bin centered at multiple L_b, $C_{L_b}^{\kappa\kappa}(\theta)$ is the theory spectrum calculated using a set of cosmological parameters θ, $\hat{C}_{L_b}^{\kappa\kappa}$ is the mock "measured" spectrum and $\mathbb{C}_{bb'}$ is the covariance matrix generated as described below.

We adopt the extended range bin configuration used in the ACT DR6 analysis, with the $N_{\text{bins}} = 18$ non-overlapping bins centered at $L = [14, 30, 53, 84, 123, 172, 232, 302, 382, 476, 582, 700, 832, 1001, 1200, 1400, 1600, 1874]$. To evaluate the impact of using a different binning scheme on the forecasted parameter constraints, we also generated mock CMB lensing datasets N_{bins} ranging from 13 to 100, with the bin widths forming an arithmetic progression resulting in progressively wider bins at higher multipoles. We found that the uncertainties in the cosmological parameters converged for the 18-bin case we have adopted.

To generate a single realization of the mock data, we use the additive Gaussian noise approximation by drawing a random sample from a Gaussian distribution centered at the fiducial cosmology $C_L^{\kappa\kappa}$ and standard deviation given by

$$\Delta C_L^{\kappa\kappa} = \sqrt{\frac{2}{f_{\text{sky}}(2L+1)}}\left(C_L^{\kappa\kappa} + N_L^{\kappa\kappa}\right),$$

(8)

where $N_L^{\kappa\kappa}$ is the noise power spectrum, and f_{sky} is the fraction of sky coverage [66]. Following the methodology described in [29], we obtain the band-power covariance matrix from $N_{\text{mock}} = 796$ mock simulations while assuming SO-like sky coverage $f_{\text{sky}} = 0.5$. To account for

the biased estimate of the covariance matrix from a finite number of realizations, we rescale the estimated inverse covariance matrix by the Hartlap factor [67]:

$$f_{\text{H}} = \frac{N_{\text{mock}} - N_{\text{bins}} - 2}{N_{\text{mock}} - 1},$$

(9)

where N_{bins} is the number of bandpowers.

As the noise power spectrum $N_L^{\kappa\kappa}$, we use the Simons Observatory minimum variance (MV) noise curve `v3.1.1` with the goal sensitivity for the large aperture telescope (LAT) [68]. The dominant contribution arises from the disconnected Gaussian term, $N^{(0)}$, which originates from random correlations in the primary CMB anisotropies [69]. Additional noise comes from instrumental and atmospheric fluctuations, which introduce anisotropic variance in the maps. Foreground contamination, including the thermal and kinetic Sunyaev–Zel'dovich effects, cosmic infrared background, and unresolved point sources, adds non-Gaussian structure that biases lensing estimators. Furthermore, masking of bright sources and survey geometry effects can induce additional biases if not properly accounted for [70].

2. 3 × 2-pt galaxy weak lensing and clustering

To model a future galaxy weak lensing and clustering dataset (w_{ij}, $\gamma_{t,ij}$, and $\xi_{\pm,ij}$), we generate mock DES-Year-1-like 3×2-pt data vectors based on our fiducial ΛCDM cosmology. We then add Gaussian noise drawn from the DES Y1 covariance matrix, rescaled by a factor of 25 to approximate the precision expected from future surveys. Our mock likelihood is based on the publicly available `Cobaya` implementation of the DES Y1 [71, 72] likelihood, with the rescaled covariance and the mock data.

For the MCMC runs with the mock SO-L CMB lensing data, we vary and marginalize over the DES-Y1 likelihood nuisance parameters. For runs combined with the CV-L CMB lensing mock, we fixed the nuisance parameters at their fiducial values. The former setup is meant to represent a combination that can be expected to be available in the relatively near future, while the latter is more representative of the ultimate limit. Throughout the paper, we denote the 3×2-pt mock analysis with fixed nuisance parameters with an asterisk, *i.e.* $3 \times 2\text{-pt}^*$, in both tables and figures.

3. BAO & SN forecast methodology

To model a future BAO dataset, we generate mock data for the three types of BAO observables D_M/r_d, D_H/r_d, and D_V/r_d based on the fiducial model and the DESI DR2 data covariance, reduced by a factor of 2. This is meant to approximate the BAO data from the completed full 14,000 deg^2 DESI program [73], which will cover approximately twice the volume included in

the DR2 release. We obtain a covariance matrix from $N_{\rm mock} = 796$ simulations, with the mock BAO estimates given as 13 data points at 7 effective redshifts: $z_{\rm eff} = [0.295, 0.510, 0.706, 0.934, 1.321, 1.484, 2.330]$, that match the redshifts in the native `Cobaya` DESI DR2 BAO likelihood and making it easy to modify it for use with our mock data.

To model a future SN Ia dataset, we adopt the Pantheon+ sample [35] as our template, computing the theoretical distance modulus, $\mu_{\rm th}(z)$, at each redshift using `CAMB` [49] for the Planck ΛCDM best-fit parameters. Mock data are then generated by adding Gaussian noise with standard deviations given by the Pantheon+ uncertainties reduced by a factor of 2.5, corresponding to an "ultimate" SN sample with roughly six times more objects than the current dataset, as expected from Vera Rubin LSST and Euclid, both of which forecast around 10^4 high-quality SN Ia [74, 75]. The mock SN sample is then binned into $N_{\rm bins} = 40$ redshift bins using an equal-occupancy (quantile) scheme, which ensures that each bin contains a comparable number of SN and thus similar statistical precision on $\mu(z_b)$. For validation, we also tested an alternative "Union3" binning scheme with fixed bin centers matching the Union3 [76] compilation.

We produce $N_{\rm mock} = 796$ independent realizations of the binned data vector $\hat{\mu}(z_b)$ and estimate the covariance matrix $\mathbb{C}_{bb'}$ from these realizations. To correct for the bias in the inverse covariance from a finite number of realizations, we rescale it by the Hartlap factor.

The resulting mock SN likelihood has the form

$$-2\ln\mathcal{L} = \sum_{bb'} [\hat{\mu}(z_b) - \mu_{\rm th}(z_b;\theta)] \, \mathbb{C}_{bb'}^{-1} \, [\hat{\mu}(z_{b'}) - \mu_{\rm th}(z_{b'};\theta)] \,,$$
(10)

where θ denotes the set of cosmological parameters.

This approach yields a mock SN likelihood that retains the statistical properties and redshift coverage of Pantheon+, but with the improved constraining power expected from Vera Rubin LSST and Euclid.

IV. RESULTS

In what follows, we present the r_d-agnostic parameter constraints inferred from the current data, as well as the forecasts. The results for the fixed and the varying Σm_ν analyses are summarized in Tables II and III, respectively, and the key parameter posteriors are shown in Figures 3 and 5. The r_d-agnostic tests are compared to the standard ΛCDM fits to the combination of DESI2 BAO, PP SN and DES Year-3 with the full complement of Planck CMB spectra, namely, the NPIPE `CamSpec` high-ℓ likelihood [77, 78], the PR4 CMB lensing [50], and the PR3 low-ℓ TT and EE [1, 79] (DESI2+Planck+DESY3+PP), where r_d was a derived parameter computed using the standard recombination routine in `CAMB`. Throughout this section, including in the tables and the figures, we refer to the

DESI2+$\theta_\star$+APS-L combination as the "Base" dataset.

A. Current data constraints with fixed Σm_ν

With r_d as a free parameter, the combination of DESI2, $\theta_\star$ and APS-L (Base) yields $H_0 = 70.5 \pm 2.0$ km/s/Mpc. Adding DESY3 improves the H_0 constraint by about 15%, with $H_0 = 70.3 \pm 1.7$ km/s/Mpc. Supplementing this with the CMB-based Gaussian prior on A_s significantly reduces the uncertainty, resulting in $H_0 = 70.40 \pm 0.98$ km/s/Mpc, while also improving the constraints on r_d and $\Omega_m h^2$.

Adding the PP SN data leads to only minor shifts in the mean values and practically no reduction in parameter uncertainties. This lack of improvement despite SN offering an independent constraint on Ω_m can be explained by the fact that PP prefers a value of Ω_m [35] that is 1.8σ higher than the one preferred by DESI2 [27]. The combination of Base+DESY3+PP+A_s yields $H_0 = 70.03 \pm 0.97$ km/s/Mpc that is 2.3σ above $H_0 = 67.69 \pm 0.35$ km/s/Mpc obtained from the conventional derived-r_d fit to DESI2+Planck+DESY3+PP, 2.4σ above the Planck-only value of $H_0 = 67.36 \pm 0.54$ km/s/Mpc and 2.1σ below the SH0ES Cepheid-based distance ladder measurement of 73.04 ± 1.04 km/s/Mpc.

The Base+DESY3+PP+A_s value of $S_8 = 0.827 \pm 0.009$ is in good agreement with $S_8 = 0.825^{+0.015}_{-0.013}$ obtained in [25] from APS-L alone, and the DESI2+Planck+DESY3+PP value of $S_8 = 0.818 \pm 0.008$.

B. Current data constraints with varying Σm_ν

Neutrinos with masses in the $[0, 3.0]$ eV range contribute as radiation at matter-radiation equality, and also suppress the growth of cosmic structure on smaller scales. Both effects affect the shape of the matter power spectrum and, consequently, the CMB lensing convergence spectrum and the galaxy lensing and clustering, making the latter a probe of the total neutrino mass.

As discussed in Sec. II D and seen in Fig. 3, there is a positive correlation between Σm_ν and $\Omega_m h^2$ driven by the need to preserve the value of $k_{\rm eq}$ for larger values of Σm_ν. With Ω_m constrained by BAO (and independently also by SN), this implies that Σm_ν is positively correlated with H_0. We find that allowing Σm_ν to vary considerably dilutes the constraint on H_0, with the combination of Base+DESY3+PP yielding $H_0 = 75.3^{+3.3}_{-4.0}$ km/s/Mpc. Adding a CMB-informed prior on A_s improves this to $H_0 = 73.9 \pm 2.2$ km/s/Mpc, while constraining the neutrino masses to $\Sigma m_\nu = 0.46^{+0.21}_{-0.25}$ eV ($0.46^{+0.40}_{-0.45}$ eV at 95% CL).

Assigning uniform probability for Σm_ν to take any value in the $[0, 3]$ eV range, with the parameter being relatively unconstrained positively correlated with H_0, tends to bias the H_0 and $\Omega_m h^2$ posteriors towards larger values. To demonstrate that this is a prior-related effect,

Current Data (fixed Σm_ν)	H_0 [km/s/Mpc]	$100\,\Omega_m h^2$	Ω_m	r_d [Mpc]	$\ln(10^{10}A_s)$	S_8
[a] DESI2+Planck+DESY3+PP	67.69 ± 0.35	14.16 ± 0.07	0.309 ± 0.005	148.6 ± 0.35	3.040 ± 0.014	0.818 ± 0.008
DESI2+$\theta_\star$+APS-L (Base)	70.5 ± 2.0	14.75 ± 0.81	0.297 ± 0.005	144.2 ± 4.0	3.039 ± 0.073	0.831 ± 0.011
Base+A_s	70.42 ± 0.99	14.71 ± 0.30	0.297 ± 0.005	144.3 ± 1.6	3.040 ± 0.019	0.830 ± 0.011
Base+DESY3	70.3 ± 1.7	14.62 ± 0.64	0.295 ± 0.005	144.7 ± 3.2	3.045 ± 0.059	0.826 ± 0.009
Base+DESY3+A_s	70.40 ± 0.98	14.65 ± 0.29	0.296 ± 0.005	144.5 ± 1.6	3.041 ± 0.019	0.826 ± 0.009
Base+DESY3+PP	70.0 ± 1.7	$14.60^{+0.60}_{-0.68}$	0.298 ± 0.005	145.0 ± 3.2	3.044 ± 0.060	0.827 ± 0.009
Base+DESY3+PP+A_s	70.03 ± 0.97	14.62 ± 0.29	0.298 ± 0.005	144.8 ± 1.6	3.041 ± 0.019	0.827 ± 0.009
Forecast (fixed Σm_ν)						
BAO+$\theta_\star$+SO-L+SN+A_s	67.40 ± 0.71	14.33 ± 0.23	0.315 ± 0.004	146.8 ± 1.3	3.037 ± 0.019	0.830 ± 0.004
BAO+$\theta_\star$+SO-L+3×2-pt+SN	$67.30^{+1.1}_{-1.2}$	$14.33^{+0.43}_{-0.51}$	0.316 ± 0.003	146.9 ± 2.5	3.037 ± 0.045	0.831 ± 0.003
BAO+$\theta_\star$+SO-L+3×2-pt+SN+A_s	67.24 ± 0.67	14.30 ± 0.22	0.316 ± 0.003	147.0 ± 1.2	3.039 ± 0.019	0.831 ± 0.003
BAO+$\theta_\star$+CV-L+SN+A_s	67.30 ± 0.70	14.37 ± 0.22	0.317 ± 0.004	147.2 ± 1.3	3.040 ± 0.019	0.835 ± 0.002
BAO+$\theta_\star$+CV-L+3×2-pt*+SN	67.10 ± 1.0	14.27 ± 0.41	0.317 ± 0.002	147.8 ± 2.2	3.051 ± 0.038	0.835 ± 0.002
BAO+$\theta_\star$+CV-L+3×2-pt*+SN+A_s	67.30 ± 0.57	14.35 ± 0.21	0.317 ± 0.002	147.3 ± 1.2	3.042 ± 0.018	0.834 ± 0.002

[a] In the analysis using the full Planck data, r_d is a derived parameter computed using the standard recombination routine in `CAMB`. In the analyses of all other data combinations in this table, r_d is a free parameter.

Table II: Constraints on cosmological parameters from current data, assuming fixed $\Sigma m_\nu = 0.06$ eV. The "Base" dataset denotes DESI2+$\theta_\star$+APS-L. Uncertainties are quoted at 68% CL.

Current Data (varying Σm_ν)	H_0 [km/s/Mpc]	$100\,\Omega_m h^2$	Ω_m	Σm_ν [eV]	$\ln(10^{10}A_s)$	S_8
[a] DESI2+Planck+DESY3+PP	$67.82^{+0.47}_{-0.39}$	14.15 ± 0.08	$0.308^{+0.005}_{-0.006}$	$< 0.052\ (0.112)$	3.038 ± 0.014	0.819 ± 0.009
Base+DESY3	$75.7^{+3.1}_{-4.2}$	$17.0^{+1.3}_{-2.0}$	0.297 ± 0.005	$0.54^{+0.23}_{-0.38}\ (1.10)$	$3.007^{+0.073}_{-0.065}$	0.821 ± 0.009
Base+DESY3+A_s	74.2 ± 2.2	16.32 ± 0.96	0.297 ± 0.005	$0.45^{+0.20}_{-0.27}\ (0.862)$	3.038 ± 0.019	0.821 ± 0.009
Base+DESY3+PP	$75.3^{+3.3}_{-4.0}$	$17.0^{+1.4}_{-1.9}$	0.299 ± 0.005	$0.55^{+0.23}_{-0.37}\ (1.11)$	3.006 ± 0.069	0.822 ± 0.009
Base+DESY3+PP+A_s	73.9 ± 2.2	16.36 ± 0.92	0.299 ± 0.005	$0.46^{+0.21}_{-0.25}(0.46^{+0.40}_{-0.45})$	3.038 ± 0.019	0.824 ± 0.010
Forecast (varying Σm_ν)						
BAO+$\theta_\star$+SO-L+SN+A_s	$69.6^{+1.6}_{-1.0}$	$15.32^{+0.64}_{-1.0}$	0.316 ± 0.004	$< 0.357\ (0.632)$	3.037 ± 0.019	0.826 ± 0.005
BAO+$\theta_\star$+SO-L+3×2-pt+SN	$67.8^{+1.2}_{-1.5}$	$14.56^{+0.48}_{-0.64}$	0.317 ± 0.003	$< 0.135\ (0.273)$	3.039 ± 0.045	0.830 ± 0.004
BAO+$\theta_\star$+SO-L+3×2-pt+SN+A_s	$67.71^{+0.84}_{-1.1}$	$14.52^{+0.31}_{-0.49}$	0.317 ± 0.003	$< 0.133\ (0.263)$	3.040 ± 0.018	0.830 ± 0.004
BAO+$\theta_\star$+CV-L+SN+A_s	$68.40^{+0.98}_{-0.76}$	$14.86^{+0.36}_{-0.76}$	0.317 ± 0.004	$< 0.188\ (0.403)$	3.037 ± 0.019	0.833 ± 0.004
BAO+$\theta_\star$+CV-L+3×2-pt*+SN	$67.9^{+1.2}_{-1.4}$	$14.62^{+0.47}_{-0.62}$	0.317 ± 0.002	$0.122^{+0.050}_{-0.081}\ (0.247)$	3.046 ± 0.038	0.833 ± 0.003
BAO+$\theta_\star$+CV-L+3×2-pt*+SN+A_s	$67.99^{+0.81}_{-0.97}$	$14.67^{+0.33}_{-0.43}$	0.317 ± 0.002	$0.123^{+0.051}_{-0.079}(0.244)$	3.041 ± 0.018	0.833 ± 0.003

[a] In the analysis using the full Planck data, r_d is a derived parameter computed using the standard recombination routine in `CAMB`. In the analyses of all other data combinations in this table, r_d is a free parameter.

Table III: Constraints on cosmological parameters from current data, allowing Σm_ν to vary. The "Base" dataset denotes DESI2+$\theta_\star$+APS-L. For Σm_ν, both 68% CL intervals and 95% CL upper bounds are shown.

in Figure 4 we show posteriors for a few data combinations while using a logarithmic prior on Σm_ν covering the $[0.001, 3]$ eV mass range. With the logarithmic prior, the combination of Base+DESY3+PP+A_s yields $H_0 = 71.5^{+1.4}_{-2.9}$ and $\Sigma m_\nu = 0.205^{+0.097}_{-0.23}$ eV at 68% CL ($0.20^{+0.46}_{-0.24}$ eV at 95% CL). These are statistically consistent with the uniform prior results, but now without the apparent bias.

The r_d-agnostic bounds on Σm_ν presented in this section are substantially weaker than those from the conventional derived-r_d analysis of the DESI DR2+$Planck$+DESY3+PP dataset, $\Sigma m_\nu < 0.052$ eV (0.112 eV at 95% CL), that are getting very close to the limit of 0.06 eV.

Notably, the constraints on S_8 derived while varying Σm_ν are effectively the same as those from the fixed Σm_ν analysis in the previous subsection, and in excellent agreement with $S_8 = 0.815^{+0.016}_{-0.021}$ obtained by the KiDS-Legacy analysis [80, 81] with fixed $\Sigma m_\nu = 0.06$ eV, and $S_8 = 0.811^{+0.022}_{-0.020}$ from the DES Year 3 joint analysis of cluster abundances, weak lensing, and galaxy clustering while varying Σm_ν.
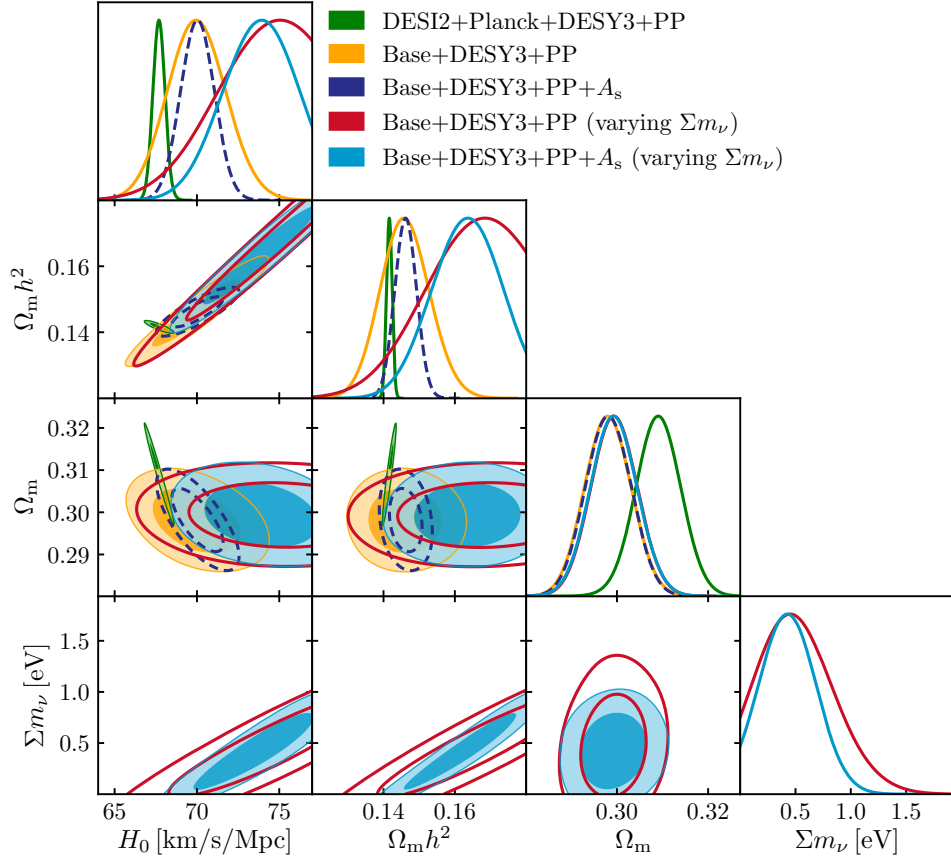
Figure 3: The 68% and 95% CL contours and the 1D marginalized posterior distributions for H_0, $\Omega_m h^2$, Ω_m, and Σm_ν from current data. The elongated 2D contours of H_0, $\Omega_m h^2$ and Σm_ν highlight the positive correlations between these parameters discussed in the text. The DESI2+Planck+DESY3+PP analysis uses the full Planck data, with r_d as a derived parameter computed using the standard recombination routine in CAMB. In the analyses of all other data combinations in this figure, r_d is a free parameter.

C. Forecasted parameter constraints

Finally, we present a forecast based on mock CMB lensing data from a Simons-Observatory-like (SO-L) experiment, a future 3×2-pt galaxy weak lensing and clustering dataset, the completed DESI BAO program, the present value of $\theta_\star$, a mock future SN sample with ~ 9000 SN magnitudes, and the same prior on A_s as the one used in the earlier subsections. We also perform the same forecast with a cosmic-variance-limited (CV-L) CMB Lensing mock data. The forecasted parameter constraints for the cases of fixed and varied Σm_ν are summarized in Tables II and III, and shown in Fig. 5. These forecasts are not meant to be an exhaustive study of the promise of the r_d-agnostic method, but rather provide a sense of what improvement one can expect over a reasonable timescale.

With a fixed Σm_ν and without an informative A_s prior, we obtain $H_0 = 67.30^{+1.1}_{-1.2}$ km/s/Mpc from the combination including the SO-L data, and $H_0 = 67.10 \pm 1.0$ km/s/Mpc from the combination with CV-L. It is interesting that eliminating the noise from the CMB lensing dataset, as in the cosmic variance limited case, leads

to almost no improvement in the constraints. This is because the uncertainty in H_0 is dominated by the remaining degeneracy between $\Omega_m h^2$ and A_s. The inclusion of the A_s prior significantly reduces the uncertainty, yielding $H_0 = 67.24 \pm 0.67$ from the combination with SO-L, and $H_0 = 67.30 \pm 0.57$ from the combination with CV-L, while also improving the constraints on other cosmological parameters. This demonstrates that the r_d-agnostic method is capable of constraining the Hubble constant at one-percent level with a realistic CMB Lensing dataset when Σm_ν is fixed.

When allowing Σm_ν to vary, we find $H_0 = 67.71^{+0.84}_{-1.1}$ km/s/Mpc and $\Sigma m_\nu < 0.133 (< 0.263)$ eV at 68% (95%) CL from the BAO+$\theta_\star$+SO-L+3 × 2-pt+SN+A_s combination, and $H_0 = 67.99^{+0.81}_{-0.97}$ km/s/Mpc and $\Sigma m_\nu = 0.123^{+0.051}_{-0.079} (< 0.244)$ eV at 68% (95%) CL from BAO+$\theta_\star$+CV-L+3 × 2-pt*+SN+A_s combination. As in the fixed Σm_ν case, the added sensitivity to small-scale suppression at high ℓ offered by the CV-L combination does not lead to a substantial improvement in constraining power, while the prior on A_s makes a notable difference.
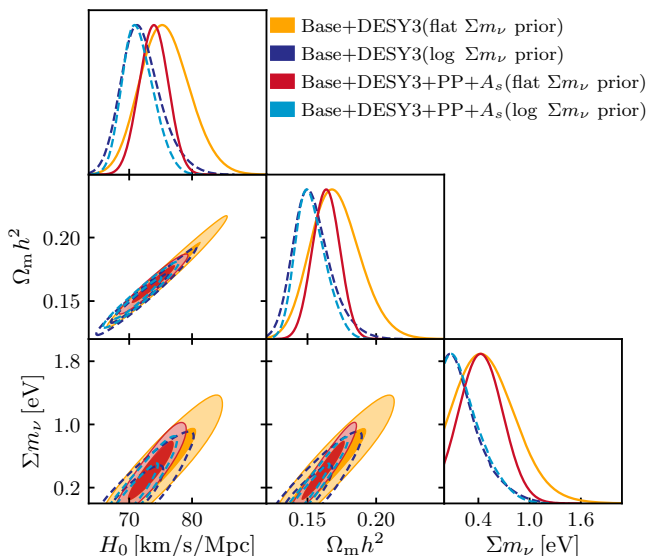
Figure 4: The 68% and 95% CL contours, along with the 1D marginalized posterior distributions for H_0, $\Omega_m h^2$, and Σm_ν from current data, comparing the results obtained with a uniform prior and a logarithmic prior on Σm_ν. This figure illustrates how using a logarithmic prior eliminates the apparent bias towards higher values of H_0 and $\Omega_m h^2$.

In the mock posteriors, we no longer see the shift to higher $\Omega_m h^2$ and H_0 values when sampling Σm_ν with a uniform prior. This is because Σm_ν is much better constrained by the mock data, reducing the dependence on the prior choice.

V. SUMMARY

The Hubble tension, and attempts to resolve it through new ingredients in early-Universe physics, motivate efforts to measure H_0 without relying on a model for the sound horizon r_d or calibrating supernovae. In this work, we combined CMB lensing measurements from ACT, *Planck*, and SPT-3G with the DES Year-3 3×2-pt galaxy weak lensing and clustering correlations, DESI DR2 BAO, the CMB acoustic scale angle $\theta_\star$, and PP SN data, while treating r_d as a free parameter.

With a conservative prior on the amplitude of primordial fluctuations A_s, we find $H_0 = 70.03 \pm 0.97$ km/s/Mpc when fixing the neutrino mass sum to its minimal value $\Sigma m_\nu = 0.06$ eV. This is 2.1σ below the SH0ES Cepheid-based distance-ladder measurement [2] and 2.4σ above the *Planck* ΛCDM value [78], consistent with alternative distance-ladder determinations [82]. Allowing Σm_ν to vary increases the uncertainty in H_0, but still yields a sub-3% r_d-agnostic constraint of $H_0 = 73.9 \pm 2.2$ km/s/Mpc.

Forecasts combining future CMB lensing data from a Simons-Observatory-like experiment, a next-generation 3×2-pt dataset, the completed DESI BAO program, $\theta_\star$, a future SN sample, and a conservative A_s prior predict $\sigma(H_0) \simeq 0.67$ km/s/Mpc. This is comparable to the precision of full-*Planck* CMB analyses, demonstrating that the sound-horizon-agnostic approach can deliver an independent and competitive test of the need for new physics at recombination.

Although our Gaussian prior on A_s was deliberately conservative, encompassing the parameter space allowed by modified recombination models with higher H_0, it will be valuable to explore whether future tomographic clustering and weak-lensing data from Vera Rubin LSST [74] and *Euclid* [83] can remove the need for such a prior. The expanded mode coverage from LSST and *Euclid* should improve sensitivity to the neutrino free-streaming suppression of growth [84] and help disentangle the effects of $\Omega_m h^2$, A_s, and Σm_ν, especially when combined with low-noise CMB lensing. We leave this for future work.
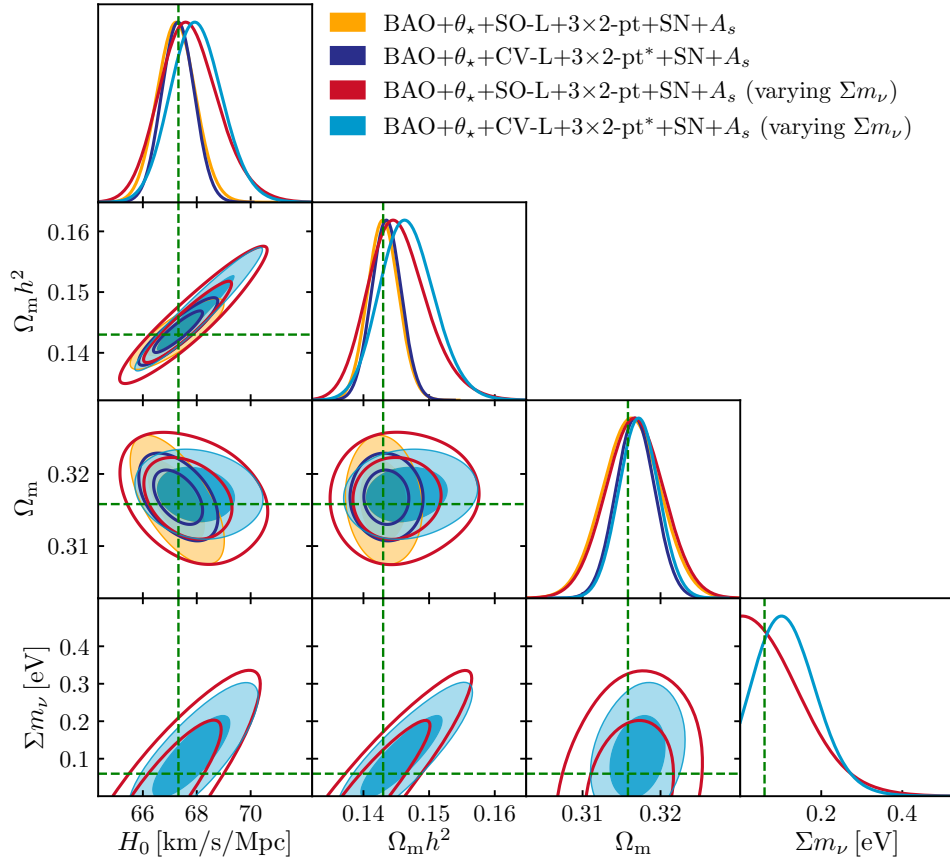
Figure 5: The forecasted 68% and 95% CL posterior distributions for H_0, $\Omega_m h^2$, Ω_m, and Σm_ν. For reference, the green dashed lines represent the fiducial values used in the forecast.

[1] N. Aghanim *et al.* (Planck), Planck 2018 results. VI. Cosmological parameters, Astron. Astrophys. **641**, A6 (2020), [Erratum: Astron.Astrophys. 652, C4 (2021)], arXiv:1807.06209 [astro-ph.CO].

[2] A. G. Riess *et al.*, A Comprehensive Measurement of the Local Value of the Hubble Constant with 1 km s^{-1} Mpc^{-1} Uncertainty from the Hubble Space Telescope and the SH0ES Team, Astrophys. J. Lett. **934**, L7 (2022), arXiv:2112.04510 [astro-ph.CO].

[3] K. Jedamzik and T. Abel, Small-scale primordial magnetic fields and anisotropies in the cosmic microwave background radiation, JCAP **10**, 050.

[4] K. Jedamzik and A. Saveliev, Stringent Limit on Primordial Magnetic Fields from the Cosmic Microwave Background Radiation, Phys. Rev. Lett. **123**, 021301 (2019), arXiv:1804.06115 [astro-ph.CO].

[5] K. Jedamzik and L. Pogosian, Relieving the Hubble tension with primordial magnetic fields, Phys. Rev. Lett. **125**, 181302 (2020), arXiv:2004.09487 [astro-ph.CO].

[6] K. Jedamzik, L. Pogosian, and T. Abel, Hints of Primordial Magnetic Fields at Recombination and Implications for the Hubble Tension, (2025), arXiv:2503.09599 [astro-ph.CO].

[7] T. Karwal and M. Kamionkowski, Dark energy at early times, the Hubble parameter, and the string axiverse, Phys. Rev. D **94**, 103523 (2016), arXiv:1608.01309 [astro-ph.CO].

[8] V. Poulin, T. L. Smith, T. Karwal, and M. Kamionkowski, Early Dark Energy Can Resolve The Hubble Tension, Phys. Rev. Lett. **122**, 221301 (2019), arXiv:1811.04083 [astro-ph.CO].

[9] T. L. Smith, V. Poulin, and M. A. Amin, Oscillating scalar fields and the Hubble tension: a resolution with novel signatures, Phys. Rev. D **101**, 063523 (2020), arXiv:1908.06995 [astro-ph.CO].

[10] J. L. Bernal, L. Verde, and A. G. Riess, The trouble with H_0, JCAP **10**, 019, arXiv:1607.05617 [astro-ph.CO].

[11] H. G. Escudero and K. N. Abazajian, Status of neutrino cosmology: Standard ΛCDM, extensions, and tensions, Phys. Rev. D **111**, 043520 (2025), arXiv:2412.05451 [astro-ph.CO].

[12] C. D. Kreisch, F.-Y. Cyr-Racine, and O. Doré, Neutrino puzzle: Anomalies, interactions, and cosmological tensions, Phys. Rev. D **101**, 123505 (2020), arXiv:1902.00534 [astro-ph.CO].

[13] S. Pan, W. Yang, E. Di Valentino, E. N. Saridakis, and S. Chakraborty, Interacting scenarios with dynamical dark energy: Observational constraints and alleviation of the H_0 tension, Phys. Rev. D **100**, 103520 (2019), arXiv:1907.07540 [astro-ph.CO].

[14] L. Hart and J. Chluba, Updated fundamental constant constraints from Planck 2018 data and possible relations to the Hubble tension, Mon. Not. Roy. Astron. Soc. **493**, 3255 (2020), arXiv:1912.03986 [astro-ph.CO].

[15] L. Hart and J. Chluba, Varying fundamental constants principal component analysis: additional hints about the Hubble tension, Mon. Not. Roy. Astron. Soc. **510**, 2206 (2022), arXiv:2107.12465 [astro-ph.CO].

[16] M. Baryakhtar, O. Simon, and Z. J. Weiner, Cosmology with varying fundamental constants from hyperlight, coupled scalars, Phys. Rev. D **110**, 083505 (2024), arXiv:2405.10358 [astro-ph.CO].

[17] E. Di Valentino, O. Mena, S. Pan, L. Visinelli, W. Yang, A. Melchiorri, D. F. Mota, A. G. Riess, and J. Silk, In the realm of the Hubble tension—a review of solutions, Class. Quant. Grav. **38**, 153001 (2021), arXiv:2103.01183 [astro-ph.CO].

[18] N. Schöneberg, G. Franco Abellán, A. Pérez Sánchez, S. J. Witte, V. Poulin, and J. Lesgourgues, The H0 Olympics: A fair ranking of proposed models, Phys. Rept. **984**, 1 (2022), arXiv:2107.10291 [astro-ph.CO].

[19] H. G. Escudero, J.-L. Kuo, R. E. Keeley, and K. N. Abazajian, Early or phantom dark energy, self-interacting, extra, or massive neutrinos, primordial magnetic fields, or a curved universe: An exploration of possible solutions to the H0 and $\sigma 8$ problems, Phys. Rev. D **106**, 103517 (2022), arXiv:2208.14435 [astro-ph.CO].

[20] O. H. E. Philcox, B. D. Sherwin, G. S. Farren, and E. J. Baxter, Determining the Hubble Constant without the Sound Horizon: Measurements from Galaxy Surveys, Phys. Rev. D **103**, 023538 (2021), arXiv:2008.08084 [astro-ph.CO].

[21] E. J. Baxter and B. D. Sherwin, Determining the Hubble Constant without the Sound Horizon Scale: Measurements from CMB Lensing, Mon. Not. Roy. Astron. Soc. **501**, 1823 (2021), arXiv:2007.04007 [astro-ph.CO].

[22] G. S. Farren, O. H. E. Philcox, and B. D. Sherwin, Determining the Hubble constant without the sound horizon: Perspectives with future galaxy surveys, Phys. Rev. D **105**, 063503 (2022), arXiv:2112.10749 [astro-ph.CO].

[23] O. H. E. Philcox, G. S. Farren, B. D. Sherwin, E. J. Baxter, and D. J. Brout, Determining the Hubble constant without the sound horizon: A 3.6% constraint on H0 from galaxy surveys, CMB lensing, and supernovae, Phys. Rev. D **106**, 063530 (2022), arXiv:2204.02984 [astro-ph.CO].

[24] E. A. Zaborowski *et al.*, A Sound Horizon-Free Measurement of H_0 in DESI 2024, JCAP **06**, 020, arXiv:2411.16677 [astro-ph.CO].

[25] F. J. Qu *et al.* (SPT-3G, ACT), Unified and consistent structure growth measurements from joint ACT, SPT and \textit{Planck} CMB lensing, (2025), arXiv:2504.20038 [astro-ph.CO].

[26] L. Pogosian, G.-B. Zhao, and K. Jedamzik, Recombination-independent determination of the sound horizon and the Hubble constant from BAO, Astrophys. J. Lett. **904**, L17 (2020), arXiv:2009.08455 [astro-ph.CO].

[27] M. Abdul Karim *et al.* (DESI), DESI DR2 Results II: Measurements of Baryon Acoustic Oscillations and Cosmological Constraints, (2025), arXiv:2503.14738 [astro-ph.CO].

[28] Y. Akrami *et al.* (Planck), *Planck* intermediate results. LVII. Joint Planck LFI and HFI data processing, Astron. Astrophys. **643**, A42 (2020), arXiv:2007.04997 [astro-ph.CO].

[29] F. J. Qu *et al.* (ACT), The Atacama Cosmology Telescope: A Measurement of the DR6 CMB Lensing Power Spectrum and Its Implications for Structure Growth, Astrophys. J. **962**, 112 (2024), arXiv:2304.05202 [astro-ph.CO].

[30] N. MacCrann *et al.* (ACT), The Atacama Cosmology Telescope: Mitigating the Impact of Extragalactic Foregrounds for the DR6 Cosmic Microwave Background Lensing Analysis, Astrophys. J. **966**, 138 (2024), arXiv:2304.05196 [astro-ph.CO].

[31] M. S. Madhavacheril *et al.* (ACT), The Atacama Cosmology Telescope: DR6 Gravitational Lensing Map and Cosmological Parameters, Astrophys. J. **962**, 113 (2024), arXiv:2304.05203 [astro-ph.CO].

[32] F. Ge *et al.* (SPT-3G), Cosmology from CMB lensing and delensed EE power spectra using 2019–2020 SPT-3G polarization data, Phys. Rev. D **111**, 083534 (2025), arXiv:2411.06000 [astro-ph.CO].

[33] T. M. C. Abbott *et al.* (DES), Dark Energy Survey Year 3 results: Cosmological constraints from galaxy clustering and weak lensing, Phys. Rev. D **105**, 023520 (2022), arXiv:2105.13549 [astro-ph.CO].

[34] T. M. C. Abbott *et al.* (DES), Dark Energy Survey Year 3 Results: Cosmological Constraints from Cluster Abundances, Weak Lensing, and Galaxy Clustering, (2025), arXiv:2503.13632 [astro-ph.CO].

[35] D. Brout *et al.*, The Pantheon+ Analysis: Cosmological Constraints, Astrophys. J. **938**, 110 (2022), arXiv:2202.04077 [astro-ph.CO].

[36] M. Abitbol *et al.* (Simons Observatory), The Simons Observatory: Science Goals and Forecasts for the Enhanced Large Aperture Telescope, (2025), arXiv:2503.00636 [astro-ph.IM].

[37] D. J. Eisenstein *et al.* (SDSS), Detection of the Baryon Acoustic Peak in the Large-Scale Correlation Function of SDSS Luminous Red Galaxies, Astrophys. J. **633**, 560 (2005), arXiv:astro-ph/0501171.

[38] G. E. Addison, D. J. Watts, C. L. Bennett, M. Halpern, G. Hinshaw, and J. L. Weiland, Elucidating ΛCDM: Impact of Baryon Acoustic Oscillation Measurements on the Hubble Constant Discrepancy, Astrophys. J. **853**, 119 (2018), arXiv:1707.06547 [astro-ph.CO].

[39] L. Pogosian, G.-B. Zhao, and K. Jedamzik, A Consistency Test of the Cosmological Model at the Epoch of Recombination Using DESI Baryonic Acoustic Oscillation and Planck Measurements, Astrophys. J. Lett. **973**, L13 (2024), arXiv:2405.20306 [astro-ph.CO].

[40] P. A. R. Ade *et al.* (Planck), Planck 2015 results. XV. Gravitational lensing, Astron. Astrophys. **594**, A15 (2016), arXiv:1502.01591 [astro-ph.CO].

[41] S. H. Mirpoorian, K. Jedamzik, and L. Pogosian, Modified recombination and the Hubble tension, Phys. Rev. D **111**, 083519 (2025), arXiv:2411.16678 [astro-ph.CO].

[42] J. DeRose *et al.* (DES), Dark Energy Survey Year 3 results: Cosmology from combined galaxy clustering and lensing validation on cosmological simulations, Phys. Rev. D **105**, 123520 (2022), arXiv:2105.13547 [astro-ph.CO].

[43] G. P. Lynch and L. Knox, What's the matter with Σm_ν?, (2025), arXiv:2503.14470 [astro-ph.CO].

[44] M. Loverde and Z. J. Weiner, Massive neutrinos and cosmic composition, JCAP **12**, 048, arXiv:2410.00090 [astro-

ph.CO].

[45] N. Craig, D. Green, J. Meyers, and S. Rajendran, No νs is Good News, (2024), arXiv:2405.00836 [astro-ph.CO].

[46] J. Torrado and A. Lewis, Cobaya: Code for Bayesian Analysis of hierarchical physical models, JCAP **05**, 057, arXiv:2005.05290 [astro-ph.IM].

[47] Z. Wang, D. Saadeh, K. Koyama, L. Pogosian, B. Bose, L. Yi, and G.-B. Zhao, Extending MGCAMB tests of gravity to nonlinear scales, JCAP **11**, 003, arXiv:2406.09204 [astro-ph.CO].

[48] D. Scolnic *et al.*, The Pantheon+ Analysis: The Full Data Set and Light-curve Release, Astrophys. J. **938**, 113 (2022), arXiv:2112.03863 [astro-ph.CO].

[49] A. Lewis, A. Challinor, and A. Lasenby, Efficient computation of CMB anisotropies in closed FRW models, Astrophys. J. **538**, 473 (2000), arXiv:astro-ph/9911177.

[50] J. Carron, M. Mirmelstein, and A. Lewis, CMB lensing from Planck PR4 maps, JCAP **09**, 039, arXiv:2206.07773 [astro-ph.CO].

[51] S. H. Mirpoorian, K. Jedamzik, and L. Pogosian, Is Dynamical Dark Energy Necessary? DESI BAO and Modified Recombination, (2025), arXiv:2504.15274 [astro-ph.CO].

[52] L. Pagano, J. M. Delouis, S. Mottet, J. L. Puget, and L. Vibert, Reionization optical depth determination from Planck HFI data with ten percent accuracy, Astron. Astrophys. **635**, A99 (2020), arXiv:1908.09856 [astro-ph.CO].

[53] N. Sailer, G. S. Farren, S. Ferraro, and M. White, Dispuτable: the high cost of a low optical depth, (2025), arXiv:2504.16932 [astro-ph.CO].

[54] R. J. Cooke, M. Pettini, and C. C. Steidel, One Percent Determination of the Primordial Deuterium Abundance, Astrophys. J. **855**, 102 (2018), arXiv:1710.11129 [astro-ph.CO].

[55] K. Eguchi *et al.* (KamLAND), First results from KamLAND: Evidence for reactor anti-neutrino disappearance, Phys. Rev. Lett. **90**, 021802 (2003), arXiv:hep-ex/0212021.

[56] D. S. Ayres *et al.* (NOvA), NOvA: Proposal to Build a 30 Kiloton Off-Axis Detector to Study $\nu_\mu \to \nu_e$ Oscillations in the NuMI Beamline, (2004), arXiv:hep-ex/0503053.

[57] Q. R. Ahmad *et al.* (SNO), Direct evidence for neutrino flavor transformation from neutral current interactions in the Sudbury Neutrino Observatory, Phys. Rev. Lett. **89**, 011301 (2002), arXiv:nucl-ex/0204008.

[58] I. Esteban, M. C. Gonzalez-Garcia, M. Maltoni, T. Schwetz, and A. Zhou, The fate of hints: updated global analysis of three-flavor neutrino oscillations, JHEP **09**, 178, arXiv:2007.14792 [hep-ph].

[59] P. F. de Salas, D. V. Forero, S. Gariazzo, P. Martínez-Miravé, O. Mena, C. A. Ternes, M. Tórtola, and J. W. F. Valle, 2020 global reassessment of the neutrino oscillation picture, JHEP **02**, 071, arXiv:2006.11237 [hep-ph].

[60] L. T. Hergt, W. J. Handley, M. P. Hobson, and A. N. Lasenby, Bayesian evidence for the tensor-to-scalar ratio r and neutrino masses m_ν: Effects of uniform vs logarithmic priors, Phys. Rev. D **103**, 123511 (2021), arXiv:2102.11511 [astro-ph.CO].

[61] S. Gariazzo, M. Archidiacono, P. F. de Salas, O. Mena, C. A. Ternes, and M. Tórtola, Neutrino masses and their ordering: Global Data, Priors and Models, JCAP **03**, 011, arXiv:1801.04946 [hep-ph].

[62] A. J. Long, M. Raveri, W. Hu, and S. Dodelson, Neutrino Mass Priors for Cosmology from Random Matrices, Phys. Rev. D **97**, 043510 (2018), arXiv:1711.08434 [astro-ph.CO].

[63] S. Gariazzo *et al.*, Neutrino mass and mass ordering: no conclusive evidence for normal ordering, JCAP **10**, 010, arXiv:2205.02195 [hep-ph].

[64] F. Simpson, R. Jimenez, C. Pena-Garay, and L. Verde, Strong Bayesian Evidence for the Normal Neutrino Hierarchy, JCAP **06**, 029, arXiv:1703.03425 [astro-ph.CO].

[65] W. Elbers, C. S. Frenk, A. Jenkins, B. Li, and S. Pascoli, Negative neutrino masses as a mirage of dark energy, Phys. Rev. D **111**, 063534 (2025), arXiv:2407.10965 [astro-ph.CO].

[66] L. Knox, Determination of inflationary observables by cosmic microwave background anisotropy experiments, Phys. Rev. D **52**, 4307 (1995), arXiv:astro-ph/9504054.

[67] J. Hartlap, P. Simon, and P. Schneider, Why your model parameter confidences might be too optimistic: Unbiased estimation of the inverse covariance matrix, Astron. Astrophys. **464**, 399 (2007), arXiv:astro-ph/0608064.

[68] P. Ade *et al.* (Simons Observatory), The Simons Observatory: Science goals and forecasts, JCAP **02**, 056, arXiv:1808.07445 [astro-ph.CO].

[69] M. S. Madhavacheril, K. M. Smith, B. D. Sherwin, and S. Naess, CMB lensing power spectrum estimation without instrument noise bias 10.1088/1475-7516/2021/05/028 (2020), arXiv:2011.02475 [astro-ph.CO].

[70] Z. Atkins *et al.*, The Atacama Cosmology Telescope: map-based noise simulations for DR6, JCAP **11**, 073, arXiv:2303.04180 [astro-ph.CO].

[71] E. Krause *et al.* (DES), Dark Energy Survey Year 1 Results: Multi-Probe Methodology and Simulated Likelihood Analyses, (2017), arXiv:1706.09359 [astro-ph.CO].

[72] T. M. C. Abbott *et al.* (DES), Dark Energy Survey Year 1 Results: Constraints on Extended Cosmological Models from Galaxy Clustering and Weak Lensing, Phys. Rev. D **99**, 123505 (2019), arXiv:1810.02499 [astro-ph.CO].

[73] A. G. Adame *et al.* (DESI), Validation of the Scientific Program for the Dark Energy Spectroscopic Instrument, Astron. J. **167**, 62 (2024), arXiv:2306.06307 [astro-ph.CO].

[74] R. Mandelbaum *et al.* (LSST Dark Energy Science), The LSST Dark Energy Science Collaboration (DESC) Science Requirements Document, (2018), arXiv:1809.01669 [astro-ph.CO].

[75] P. Astier *et al.*, Extending the supernova Hubble diagram to z $\sim$ 1.5 with the Euclid space mission, Astron. Astrophys. **572**, A80 (2014), arXiv:1409.8562 [astro-ph.CO].

[76] D. Rubin *et al.*, Union Through UNITY: Cosmology with 2,000 SNe Using a Unified Bayesian Framework, (2023), arXiv:2311.12098 [astro-ph.CO].

[77] G. Efstathiou and S. Gratton, A Detailed Description of the CamSpec Likelihood Pipeline and a Reanalysis of the Planck High Frequency Maps **4**, 10.21105/astro.1910.00483 (2019), arXiv:1910.00483 [astro-ph.CO].

[78] E. Rosenberg, S. Gratton, and G. Efstathiou, CMB power spectra and cosmological parameters from Planck PR4 with CamSpec, Mon. Not. Roy. Astron. Soc. **517**, 4620 (2022), arXiv:2205.10869 [astro-ph.CO].

[79] N. Aghanim *et al.* (Planck), Planck 2018 results. V. CMB power spectra and likelihoods, Astron. Astrophys. **641**, A5 (2020), arXiv:1907.12875 [astro-ph.CO].

[80] B. Stölzner *et al.*, KiDS-Legacy: Consistency of cosmic

shear measurements and joint cosmological constraints with external probes, (2025), arXiv:2503.19442 [astro-ph.CO].

[81] A. H. Wright *et al.*, KiDS-Legacy: Cosmological constraints from cosmic shear with the complete Kilo-Degree Survey, (2025), arXiv:2503.19441 [astro-ph.CO].

[82] W. L. Freedman, B. F. Madore, T. J. Hoyt, I. S. Jang, A. J. Lee, and K. A. Owens, Status Report on the Chicago-Carnegie Hubble Program (CCHP): Measurement of the Hubble Constant Using the Hubble and James Webb Space Telescopes, Astrophys. J. **985**, 203 (2025), arXiv:2408.06153 [astro-ph.CO].

[83] L. Amendola *et al.*, Cosmology and fundamental physics with the Euclid satellite, Living Rev. Rel. **21**, 2 (2018), arXiv:1606.00180 [astro-ph.CO].

[84] S. Mishra-Sharma, D. Alonso, and J. Dunkley, Neutrino masses and beyond-ΛCDM cosmology with LSST and future CMB experiments, Phys. Rev. D **97**, 123544 (2018), arXiv:1803.07561 [astro-ph.CO].